RESEARCH ARTICLE

Structural and Functional Analysis of the Pore-Forming Toxin NetB from *Clostridium perfringens*

Xu-Xia Yan,[a] Corrine J. Porter,[b] Simon P. Hardy,[c] David Steer,[b] A. Ian Smith,[b] Noelene S. Quinsey,[d] Victoria Hughes,[b] Jackie K. Cheung,[a] Anthony L. Keyburn,[a,e] Magne Kaldhusdal,[c] Robert J. Moore,[a,e] Trudi L. Bannam,[a] James C. Whisstock,[b] Julian I. Rood[a]

Australian Research Council Centre of Excellence in Structural and Functional Microbial Genomics, Department of Microbiology, Monash University, Melbourne, Victoria, Australia[a]; Australian Research Council Centre of Excellence in Structural and Functional Microbial Genomics, Department of Biochemistry and Molecular Biology, Monash University, Melbourne, Victoria, Australia[b]; Norwegian Veterinary Institute, Oslo, Norway[c]; Protein Production Unit, Department of Biochemistry and Molecular Biology, Monash University, Melbourne, Victoria, Australia[d]; CSIRO Livestock Industries, Australian Animal Health Laboratory, Geelong, Victoria, Australia[e]

X.-X.Y. and C.J.P. contributed equally to the research and are joint first authors. J.C.W. and J.I.R. contributed equally to the research and are joint senior authors.

ABSTRACT *Clostridium perfringens* is an anaerobic bacterium that causes numerous important human and animal diseases, primarily as a result of its ability to produce many different protein toxins. In chickens, *C. perfringens* causes necrotic enteritis, a disease of economic importance to the worldwide poultry industry. The secreted pore-forming toxin NetB is a key virulence factor in the pathogenesis of avian necrotic enteritis and is similar to alpha-hemolysin, a β-barrel pore-forming toxin from *Staphylococcus aureus*. To address the molecular mechanisms underlying NetB-mediated tissue damage, we determined the crystal structure of the monomeric form of NetB to 1.8 Å. Structural comparisons with other members of the alpha-hemolysin family revealed significant differences in the conformation of the membrane binding domain. These data suggested that NetB may recognize different membrane receptors or use a different mechanism for membrane-protein interactions. Consistent with this idea, electrophysiological experiments with planar lipid bilayers revealed that NetB formed pores with much larger single-channel conductance than alpha-hemolysin. Channel conductance varied with phospholipid net charge. Furthermore, NetB differed in its ion selectivity, preferring cations over anions. Using hemolysis as a screen, we carried out a random-mutagenesis study that identified several residues that are critical for NetB-induced cell lysis. Mapping of these residues onto the crystal structure revealed that they were clustered in regions predicted to be required for oligomerization or membrane binding. Together these data provide an insight into the mechanism of NetB-mediated pore formation and will contribute to our understanding of the mode of action of this important toxin.

IMPORTANCE Necrotic enteritis is an economically important disease of the worldwide poultry industry and is mediated by *Clostridium perfringens* strains that produce NetB, a β-pore-forming toxin. We carried out structural and functional studies of NetB to provide a mechanistic insight into its mode of action and to assist in the development of a necrotic enteritis vaccine. We determined the structure of the monomeric form of NetB to 1.8 Å, used both site-directed and random mutagenesis to identify key residues that are required for its biological activity, and analyzed pore formation by NetB and its substitution-containing derivatives in planar lipid bilayers.

Address correspondence to Julian I. Rood, julian.rood@monash.edu, or James C. Whisstock, james.whisstock@monash.edu.

Pore-forming toxins (PFTs) are a diverse group of cytolytic proteins that are produced by many different organisms (1, 2). Bacterial PFTs are important virulence factors (1) and in general are produced as soluble precursors that bind to the host cell membrane and assemble as oligomers that subsequently form transmembrane pores (3, 4).

PFTs can be divided into two classes depending on whether the pore is formed from a β- or an α-barrel (5). The aerolysin-like β-PFT family includes aerolysin from *Aeromonas hydrophila*, *Clostridium septicum* alpha-toxin, and epsilon-toxin and enterotoxin (CPE) from *Clostridium perfringens*. The crystal structures of aerolysin (6), epsilon-toxin (7, 8), and CPE (9) are closely re-

lated. The prototype of the second family of β-PFTs is alpha-toxin or alpha-hemolysin from *Staphylococcus aureus*. The alpha-hemolysin pore consists of a heptameric structure that contains bilayer-spanning antiparallel β-barrels (10). The bacterial toxins assigned to this class include the Panton-Valentine leukocidin S toxin of *S. aureus* (11), the bicomponent staphylococcal gamma-hemolysin (12), CytK from *Bacillus cereus* (13), and beta-toxin (14) and NetB toxin from *C. perfringens* (15).

NetB toxin is involved in the pathogenesis of avian necrotic enteritis, an economically significant disease of poultry (15, 16). Genetic studies showed that a *netB* null mutant was avirulent in a chicken necrotic enteritis model and that virulence was restored
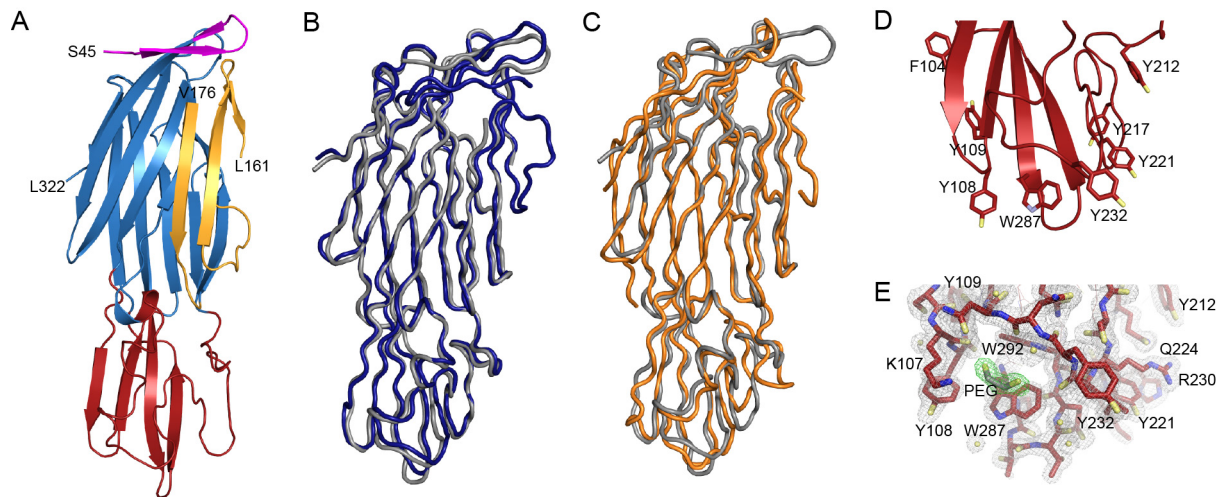
FIG 1 The 1.8-Å crystal structure of NetB. (A) Cartoon representation of the overall fold of NetB. The amino latch domain is shown in magenta, the β-sandwich domain is shown in blue, the rim domain is shown in red, and the prestem region is shown in gold. The N- and C-terminal residues are labeled. Residues 162 to 175 were not observed in the crystal structure. (B) Structural comparison of NetB (gray) with delta-toxin from *C. perfringens* (blue) (PDB ID 2YGT). (C) Structural comparison of NetB (gray) with leukocidin F (HlgB) from *S. aureus* (orange) (PDB ID 2LKF [18]). (D) Cartoon representation of the rim domain of NetB. The side chains of exposed aromatic residues are shown in stick representation and labeled. Carbon atoms are colored red, oxygen atoms are colored yellow, and nitrogen atoms are colored blue. (E) Electron density of the NetB rim domain contoured at 1 sigma (1.8-Å-resolution data). The ethylene glycol molecule that crystallized with NetB is shown in stick representation, and surrounding electron density is colored green. Residues predicted to be involved in membrane recognition are shown in stick representation. Carbon atoms are red, oxygen atoms are yellow, and nitrogen atoms are blue.

upon complementation with the wild-type *netB* gene. Comparative analysis predicted that NetB was a β-pore-forming toxin with 30% amino acid sequence identity to the alpha-hemolysin of *S. aureus*. Osmotic protection data were consistent with NetB forming pores of approximately 1.6 to 1.8 nm in chicken hepatocyte (LMH) tissue culture cells (15).

In the present study, we used a multidisciplinary approach to analyze structure-function relationships in the NetB toxin. We determined the crystal structure of the water-soluble form of NetB to 1.8 Å and showed that it adopts a fold similar to that of alpha-hemolysin. The pore-forming ability of recombinant NetB was demonstrated electrophysiologically in planar lipid bilayers. Using the ability of NetB to lyse red blood cells as a screen, we carried out a random mutagenesis study that identified several residues that were critical for NetB-induced cell lysis. Mapping of these residues onto the crystal structure revealed that they were clustered in regions predicted to be required for oligomerization and membrane binding.

RESULTS

Determination of crystal structure of NetB. NetB crystallized in space group *C2* with one molecule in the asymmetric unit. The structure of NetB was determined using molecular replacement and refined to a resolution of 1.8 Å. The final model has an *R* factor of 16.8% and an R_{free} value of 20.5% (see Table S1 in the supplemental material for structure refinement statistics). Interpretable electron density was observed for residues 45 to 161 and 176 to 322. Residues 162 to 175 were disordered and therefore not included in the final model. Note that all NetB amino acid numbers refer to the full-length NetB protein.

NetB adopts an overall β-rich fold (Fig. 1A) that is similar to that of alpha-hemolysin from *S. aureus*. The molecule consists of 16 β-strands and an α-helix, which are arranged into the

β-sandwich, latch, rim, and prestem domains that are characteristic of the alpha-hemolysin family (10, 17). Briefly, the β-sandwich domain comprises a five-stranded and a six-stranded anti-parallel β-sheet. The prestem region (residues 140 to 186) forms a three-stranded antiparallel β-sheet, which packs against the five-stranded antiparallel β-sheet of the β-sandwich (Fig. 1A). The rim region, which is involved in membrane recognition and binding, comprises a four-stranded antiparallel β-sheet and a well-ordered loop formed by residues 205 to 242. The base of the rim domain (Fig. 1D and E) contains a number of solvent-exposed aromatic groups, including F104, Y108, Y109, Y212, Y217, Y221 and Y232, and it is predicted that these residues form direct contacts with the lipid membrane. A region of uninterruptable positive density, which has been modeled as ethylene glycol, is observed in a shallow pocket at the base of the rim domain. The pocket is bounded by the side chains of K107, Y108, N234, W287, and W292.

Structural alignments and Dali searches revealed that the structure of NetB is most similar to the monomer form of the delta-toxin from *C. perfringens* (2YGT [unpublished]; root mean squared deviation [RMSD], 1.26 Å over 256 Cα [Fig. 1B]), as well as the soluble forms of staphylococcal leukocidin F (2LKF [18]; RMSD, 1.71 Å over 262 Cα [Fig. 1C]), *S. aureus* Panton-Valentine leukocidin S (1T5R [19]; RMSD, 1.65 Å over 239 Cα), and *S. aureus* leukotoxin LukE (3ROH [unpublished]; RMSD, 1.85 over 240 Cα). Comparisons with known family members revealed that NetB contains a four-residue deletion in the rim domain between D210 and G211. In LukF-PV, the additional four residues, which include W177, form part of a binding site for a phospholipid head group (18). Similarly, in alpha-hemolysin, the equivalent residues, including W179, also form a lipid-binding site (20). As a result of the four-residue deletion in NetB, the lipid head group binding site is more open and forms a groove rather than a pocket
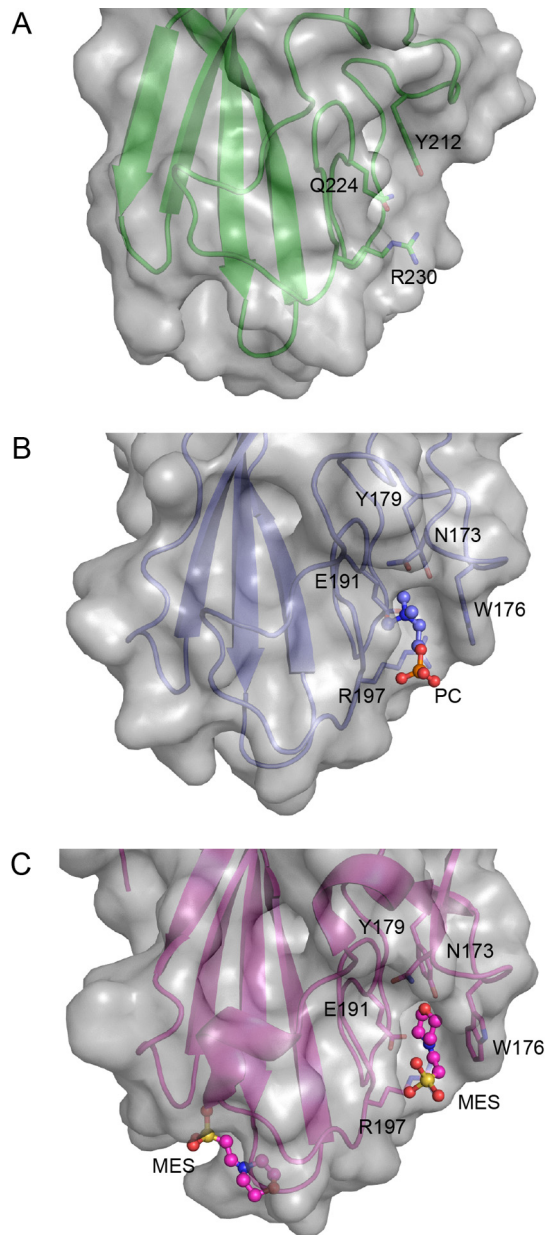
FIG 2 Structural comparison of the rim domain of NetB with HlgB and LukF-PV. Ribbon and surface representation of the rim domains of NetB (A), leukocidin F (HlgB) from *S. aureus* (PDB ID 2LKF [18]) (B), and Panton-Valentine leukocidin F (Luk-PV) from *S. aureus* (1PVL [54]) (C). The phosphocholine head group (PC) and morpholineethanesulfonic acid (MES) molecules, which crystallized with HlgB and LukF-PV, respectively, are shown in ball-and-stick representation. The residues forming the phospholipid or equivalent MES binding site are shown in stick representation. The equivalent residues in NetB are also shown in stick representation. Carbon atoms are shown in green (NetB), purple (HlgB), and pink (LukF-PV). Nitrogen atoms are shown in blue, oxygen atoms are shown in red, and sulfur atoms are shown in yellow. The format of the figure is partly based on Fig. 4 of reference 19.

(Fig. 2). As discussed below, it is anticipated that this difference may impact target recognition by the NetB toxin.

Use of mutagenesis studies to identify essential NetB residues. To determine the NetB residues that were essential for its biological function, we initially identified sites at which previous
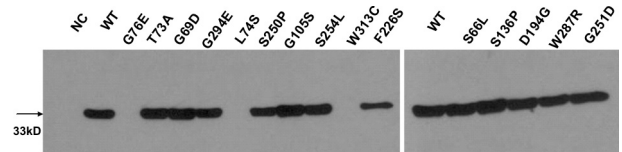

FIG 3 Western blot analysis of the random NetB substitution derivatives. Culture supernatants of late-logarithmic-phase TPG (described in the supplemental material) cultures of *C. perfringens* strains producing the NetB derivatives indicated were subjected to 12% SDS-PAGE, transferred to a nitrocellulose membrane, and Western blotted with polyclonal rabbit anti-NetB antiserum. NC, negative control; WT, wild-type strain.

mutagenesis studies had led to the inactivation of alpha-hemolysin from *S. aureus* (21) or β-toxin from *C. perfringens* (22, 23). Site-directed mutagenesis was used to make similar substitutions in NetB, specifically D186N, which replicated the β-toxin D167N substitution, and R230Q, which was comparable to the R200Q substitution in alpha-hemolysin and R212Q in β-toxin. The resultant *netB* mutants were then subcloned into a *C. perfringens-Escherichia coli* shuttle vector and introduced into several nonhemolytic *C. perfringens* strains. Since we had observed that NetB lysed horse red blood cells (RBC), hemolysis on horse blood agar (HBA) was used as a rapid functional assay for NetB activity. The results showed that although the $NetB_{R230Q}$ derivative was nonhemolytic, as expected, the $NetB_{D186N}$ toxin was still functional. Western blots confirmed that the latter still produced an immunoreactive NetB protein (data not shown).

These results showed that it was not possible to elucidate the essential NetB residues with certainty by comparative sequence analysis. Therefore, we decided to use a random mutagenesis approach to isolate nonfunctional *netB* mutants. A shuttle plasmid carrying the *netB* gene was passaged through *E. coli* mutator strain XL-1 Red. Transformation of the nonhemolytic *C. perfringens* mutant JIR4444 (24) with the *netB*$^+$ shuttle plasmid resulted in a hemolytic phenotype on HBA, with *netB* mutants detected as nonhemolytic colonies.

From many independent mutagenesis and transformation experiments, 262 potential nonhemolytic *netB* mutants were detected, 194 of which were characterized by PCR analysis and DNA sequencing. Sixty-six independent mutants were obtained; 4 had mutations in the promoter region, and 62 had mutations in the *netB* coding region. The mutated genes encoded either truncated NetB proteins of various sizes (34 independent truncated mutants [Fig. S1]) or NetB proteins with amino acid substitutions. We isolated 15 independent point mutants with only one amino acid change in the resultant NetB protein. These substitutions were evenly distributed throughout the NetB protein (see Fig. S2 in the supplemental material), although there did not appear to be any substitutions in the stem region. Western blotting of JIR4444-derived culture supernatants confirmed that 12 of these mutants produced a stable immunoreactive NetB protein of the correct molecular size (Fig. 3). The remaining NetB derivatives, L74S, G76E, and W313C NetB, were either unstable or no longer immunoreactive and therefore were not studied further.

NetB is highly active against chicken and duck red blood cells. To quantitatively measure the lytic NetB activities of the substitution-containing derivatives, we initially used horse RBC, but relatively low levels of activity were obtained. Therefore, since NetB is produced almost exclusively in *C. perfringens* strains of
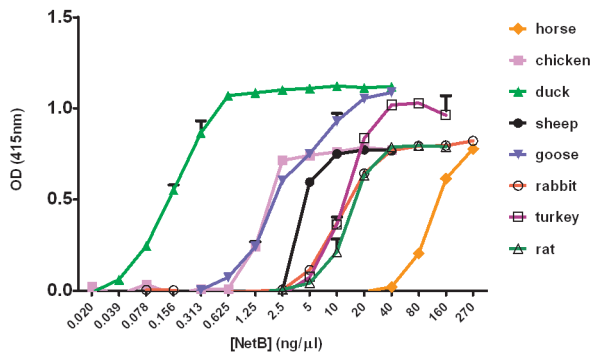
FIG 4 Quantitative analysis of hemolytic activity of NetB. Purified NetB was serially diluted 2-fold in microtiter trays and incubated at 37°C for 30 min with RBC from the eight species indicated. The release of hemoglobin was measured by the increase in optical density at 415 nm, corrected for the buffer-only negative controls. Standard deviations for triplicate experiments were calculated.

avian origin (15, 25, 26), we postulated that NetB may be more active against RBC from avian species. To examine this hypothesis, the JIR4444 derivative carrying the wild-type *netB* gene was subcultured on HBA, chicken blood agar (CBA), and duck blood agar (DBA). After overnight incubation at 37°C, more extensive hemolysis was observed on CBA and DBA than on HBA (data not shown). Titration of purified NetB against RBC from a range of animal and avian species (Fig. 4) confirmed our initial observations and showed that NetB was most active against duck, goose, and chicken RBC, with least activity observed against horse RBC.

We next purified a selection of the substitution-containing NetB proteins (G69D, T73A, D194G, S136P, R230Q, S254L, and W287R NetB) (see Fig. S2 in the supplemental material) and, based on the earlier results, quantitatively compared their activities on chicken and duck RBC to that of purified wild-type NetB. In addition, based on our analysis of the crystal structure of NetB, it was decided to clone two additional site-directed mutations, K107A and Y108A, into the *E. coli* expression vector and to purify the resultant proteins. These residues were located in the rim region of the protein and therefore were potentially involved in receptor binding. Analysis of the CD spectra of the nine purified NetB-derived proteins confirmed that they were folded and were primarily in a β-sheet conformation, as revealed from the NetB crystal structure. Quantitative analysis of the activities of these NetB derivatives showed that as expected, most of the mutants were less active than wild-type NetB (Fig. 5). One of the substitution-containing NetB proteins, S254L NetB, had no significant hemolytic activity against chicken or duck RBC, with the R230Q and W287R derivatives having very low-level activity against duck RBC and no activity against chicken RBC. The R230 and W287 residues were located in the rim region (Fig. 6) and are postulated to be involved in receptor binding. S254 was located at the interface of the main β-sandwich domain (Fig. 6) and is most likely to be involved in oligomerization. Note that mass spectrometry confirmed that the purified R230Q, S254L, and W287R proteins had the predicted amino acid substitutions.

The S254L mutant is defective in homooligomerization in solution. Analysis of purified NetB by SDS-PAGE and Western blotting revealed the presence of both monomeric and oligomeric forms of the toxin (Fig. 7). Similar profiles were observed with the
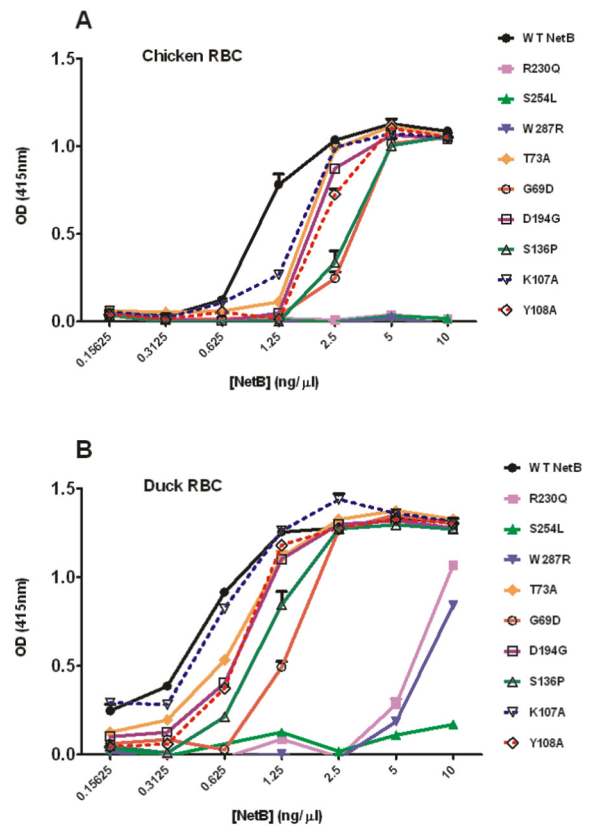

FIG 5 Quantitative hemolytic activities of substitution-containing NetB derivatives on chicken and duck RBC. The purified recombinant NetB proteins indicated were serially diluted 2-fold in microtiter trays and incubated at 37°C for 30 min with either chicken (A) or duck (B) RBC. The release of hemoglobin was measured by the increase in optical density at 415 nm, corrected for the buffer-only negative controls. Standard deviations for triplicate experiments were calculated.

R230Q and W287R derivatives, which was consistent with the hypothesis that these substitutions altered receptor binding and not oligomerization. In contrast, the nonfunctional S254L derivative of NetB did not form oligomers in solution. Similar results were observed with the S136P derivative, which lysed chicken RBC at lower efficiency than wild-type NetB. These data support the idea that these residues are required for NetB oligomerization. Note that attempts were made to identify oligomeric forms of NetB that formed in the presence of chicken RBC. No such oligomers could be detected because of masking by NetB oligomers formed in solution. No oligomers were detected when the S254L derivative was incubated with chicken RBC (data not shown).

NetB forms channels in planar phospholipid bilayers. The ability of NetB to form single channels in planar phospholipid bilayers was examined. The addition of approximately 2 μg of purified NetB to the ground bathing solution (500 μl) induced stepwise single-channel events (Fig. 8A to C). A frequency histogram of the step increases in current is shown in Fig. 8D. The mean single-channel conductance was 350 ± 10 pS. Current usually remained open, with only occasional and brief "closed" events. The current-voltage relationship appeared to be essentially linear between ±40 mV, but a tendency to close at depolarizing potentials was observed (see Fig. S3 in the supplemental material).
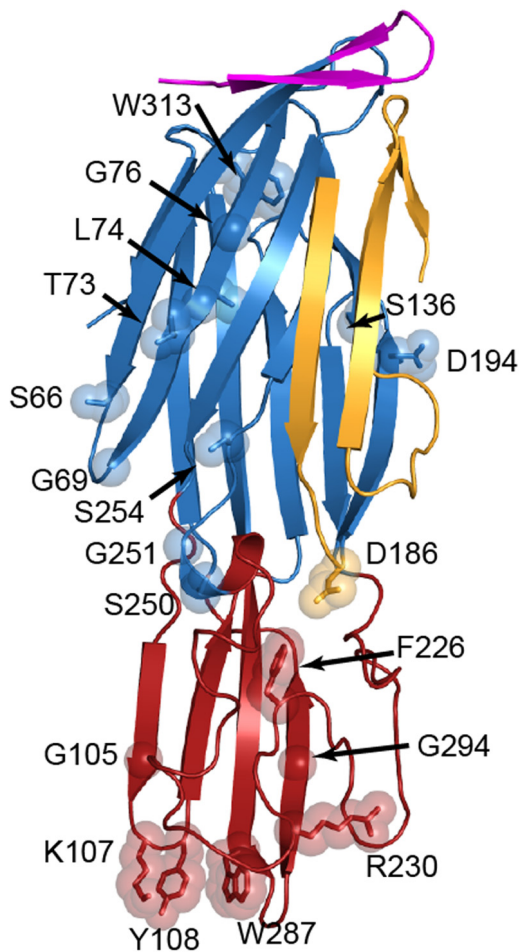
FIG 6 Cartoon representation of NetB indicating the location of the random and site-directed mutations. The side chains of the mutated residues are labeled and shown in stick and semitransparent sphere representation. The amino latch domain is shown in magenta, the β-sandwich domain is shown in blue, the rim domain is shown in red, and the prestem region is shown in gold.

The selectivity of NetB for different ions was examined in various 0.1 M salt solutions. The results (Fig. 8E) showed that the greatest reduction in mean conductance was obtained by replacing potassium with choline, indicating that the pore had a prefer-
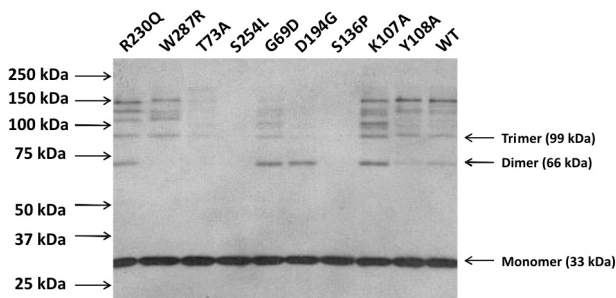

FIG 7 Oligomerization of NetB and its derivatives. The purified recombinant NetB derivatives indicated (750 ng) were separated by electrophoresis in 8% SDS-PAGE and Western blotted with polyclonal rabbit anti-NetB antiserum. The locations of size standards are indicated by the arrows on the left.

ence for cations over anions. This conclusion was confirmed by the reversal potentials obtained in asymmetric KCl solutions (see Fig. S3). NetB yielded negative reversal potentials (mean value of -17 mV $\pm$ 1 mV standard error [SE]; $n = 24$), consistent with a preference for cations, which equates to a permeability ratio (P_{cation}/P_{anion}) of 3.2. In contrast, alpha-hemolysin gave positive reversal potentials, equating to a P_{anion}/P_{cation} ratio of 1.2, a value comparable to the value of 1.5 obtained previously (27). If the weak preference of NetB for cations over anions was due to electrostatic attraction to negatively charged residues within the channel lumen, acidification of the bulk solution would tend to neutralize this effect. The data (see Fig. S2B in the supplemental material) showed that the reduction of pH to 5.0 correspondingly reduced the single-channel conductance, whereas at pH 8.5 the conductance increased.

The effect of phospholipid charge on channel conductance in 0.1 M KCl at pH 7.0 also was examined. Replacing palmitoyl-oleoylphosphatidylserine (PS) (net negative charge) with 1,2-diphytanoyl-glycero-3-phosphocholine (PC) (net positive charge) resulted in a reduction in mean channel conductance for both the NetB protein (225 $\pm$ 7 pS in palmitoyl-oleoylphosphatidylethanolamine [PE]-PC versus 325 $\pm$ 10 pS in PE-PS) and the purified W287R derivative of NetB (242 $\pm$ 10 pS in PE-PC versus 356 $\pm$ 21 pS in PE-PS). The opposite effect was observed with alpha-hemolysin, with single-channel conductance increasing from 85 $\pm$ 2 pS in PE-PS to 105 $\pm$ 3 pS in PE-PC). Pore formation could readily be detected in a selection of purified NetB substitution derivatives, with mean conductance values in 0.1 M KCl as follows: W287R derivative, 356 $\pm$ 21 pS; R230Q derivative, 356 $\pm$ 21 pS; S136P derivative, 418 $\pm$ 20 pS; K107A derivative, 311 $\pm$ 22 pS. These values were similar to that of wild-type NetB. However, the S254L derivative was essentially inactive, with channel formation occurring very rarely, even at 8 μg/ml.

DISCUSSION

Necrotic enteritis is an important disease of commercial poultry, especially with increasing constraints on the prophylactic use of antimicrobial agents in animal feeds (28). The pathogenesis of this disease is complex and remains partially unresolved (16, 26, 29), but NetB is the primary toxin involved in the disease process (15, 16). We have now determined the crystal structure of NetB, identified residues that are essential for NetB function, and mapped these residues onto the NetB structure.

Little is known about the cells that are targeted by NetB in an intestinal infection. Initial studies tested a range of cell lines for their susceptibility to NetB, but cytopathic effects were detected only on chicken LMH cells (15). In the current work, we have shown that NetB lyses horse RBC, and we used lytic activity on HBA to screen for *netB* mutants generated by random mutagenesis. We subsequently showed that NetB was much more active on avian RBC; chicken, duck, and goose RBC all had greatly increased susceptibility to NetB-mediated lysis. The reason for this increased susceptibility is not known, it is possible that avian RBC membranes have increased levels of a cell surface receptor that is required for NetB binding and its subsequent cytolytic activity or that it may reflect differences in phospholipid composition in differing animal species.

Until recently, the structures of only two β-pore-forming toxins from *C. perfringens* had been published, namely, the aerolysin-like epsilon-toxin (7, 30) and CPE (9, 31). In addition, the struc-
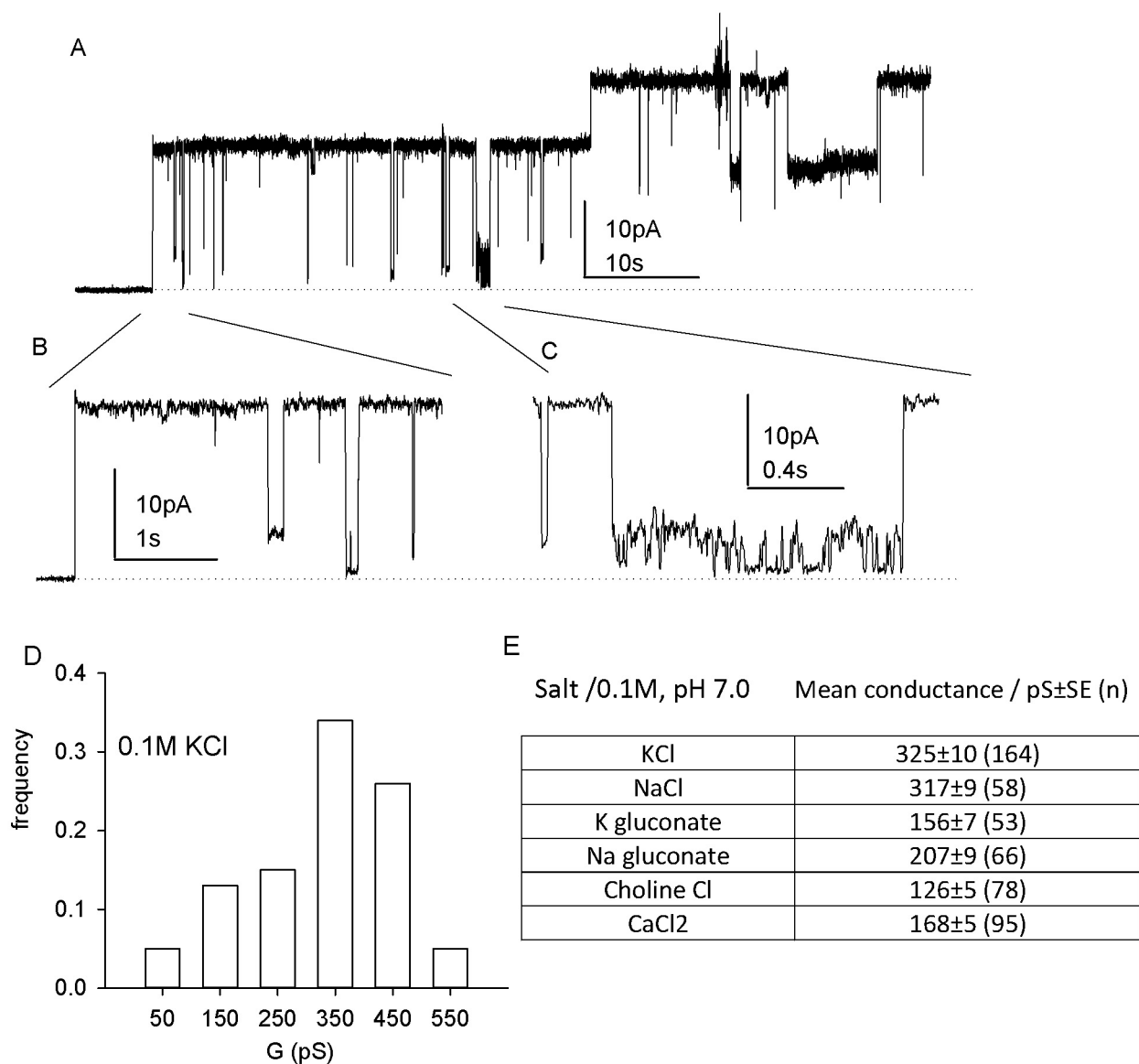
FIG 8 NetB in planar lipid bilayers. (A) Representative single-channel events recorded after addition of NetB (2 µg) to a PE-PS bilayer bathed in 0.1 M KCl and held at +40 mV. (B and C) Expanded time scales of two sections of panel A. Note the variation in closed levels in panel B and the small "flickery" events of 50 to 90 pS in panel C. (D) Distribution of mean conductance values obtained for NetB. (E) Effect of ion replacement on mean conductance values.

ture of *C. perfringens* alpha-hemolysin-like delta-toxin has been deposited in the protein structure database (2YGT). Analysis of the structure of NetB indicates that it is closely related to the alpha-hemolysin family of toxins. These toxins generally form heptameric pores in the host cell membrane, and it is highly likely that NetB also forms heptameric pores on its target cell membranes.

Initial comparative sequence analysis of NetB led to the identification of D186 and R230 as residues that were likely to be of functional importance. However, site-directed mutagenesis of these residues revealed that a D186N substitution derivative was still functional. Therefore, random mutagenesis was used to identify 12 single-amino-acid substitutions that produced a stable NetB protein in *C. perfringens* and which were nonhemolytic on HBA. Subsequent analysis on more sensitive chicken RBC, using

purified proteins, revealed that seven of these derivatives were less active than the wild-type toxin. Three of these NetB proteins, including the original R230Q derivative, were inactive against chicken RBC. The R230Q and W287R proteins were correctly folded, as determined by circular dichroism spectrometry, still formed oligomers in solution, and were able to form single channels in artificial phospholipid bilayers. Since the R230 and W287 residues are located in the putative rim domain of NetB, we postulate that these residues are required for binding to a cell surface receptor.

Unlike the other NetB substitution derivatives, the T73A, S136P, and S254L proteins all failed to form oligomers in solution. However, both the T73A and S136P proteins had reduced but significant hemolytic activity against chicken RBC, and S136P was still functional in the phospholipid bilayer assay, indicating that

these residues are involved in determining the rate of spontaneous oligomerization of NetB in solution (i.e., in the absence of red cell or synthetic membranes). We suggest that these derivatives still are able to oligomerize on the surfaces of their target avian cells. In contrast, the NetB S254L derivative was unable to oligomerize and was nonfunctional in both the chicken RBC and lipid bilayer assays. In addition, comparative analysis of the NetB structure suggests that S254 is located in the NetB domain postulated to be involved in oligomerization. Therefore, we postulate that the S254 residue of NetB is essential for the formation of a functional oligomer on the surface of the target cell. The abolition of pore-forming ability by the S254L substitution is consistent with its impaired ability to oligomerize. The fact that we could detect single channels in the other four mutants tested is consistent with the substitutions lying outside the pore lumen.

The planar lipid bilayer data demonstrate that NetB has intrinsic pore-forming activity consistent with the predicted amino acid similarity to other β-pore-forming toxins. Our data also show that the electrophysiological features of NetB have both similarities to and differences from those of *S. aureus* alpha-hemolysin, the PFT that has been best characterized in terms of both structure and electrophysiology. Channels formed by both NetB and alpha-hemolysin tend to remain in the open state and exhibit a tendency to close at positive voltages over +40 V. However, NetB channels are roughly 3-fold larger in conductance than those of alpha-hemolysin (27, 32). While alpha-hemolysin has a weak preference for anions, NetB channels exhibited a preference for cations over anions, a finding demonstrated using three experimental approaches, namely, ion replacement, reversal potential, and pH dependence. This property resembles that of a close ortholog of NetB, β-toxin from *C. perfringens*, which also preferentially conducts cations over anions (33, 34). Our analysis of the NetB structure and that of other workers (35) indicate that there are regions of electronegativity at both ends of the pore, which could select for cations. Significant differences in the channel conductance of NetB and alpha-hemolysin also were observed with the two phospholipids tested, phosphatidylcholine and phosphatidylserine. This result may reflect, at least in part, the amino acid sequence differences in the membrane-binding domain and the relative hemolytic potencies in the red cells from different animal species.

After this article was submitted for review, other workers (35) reported on the molecular architecture of the NetB pore. The structure of the heptameric pore in a detergent additive, without the first 20 amino acids of mature NetB, was solved to a resolution of 3.9 Å. They did not determine the structure of soluble monomeric NetB. They also showed that NetB interacts directly with cholesterol in the target cell membrane as part of the oligomerization and pore-forming process. Since bird and mammalian RBC have similar proportions of membrane cholesterol (36, 37), the different susceptibilities of bird and mammalian RBC to NetB-mediated lysis observed in our study do not appear to result from major differences in cholesterol levels. Mutants equivalent to our R230Q (R200A; these authors numbered the residues based on the processed NetB protein) and W287R (W257A) derivatives were constructed and analyzed. Their results were in agreement with those of our studies, since their R200A and W257A mutants had reduced cytotoxic activity compared to that of wild-type NetB.

There is a need for new vaccines that can be used for the control and prevention of necrotic enteritis in poultry (38–40). The most cost-effective necrotic enteritis vaccine may well be a live attenuated vaccine that is used in hens rather than commercial broilers. Such a vaccine may require the use of nontoxic, but immunogenic, derivatives of NetB in addition to other *C. perfringens* antigens. The R230Q, S254L, and W287R substitution-containing NetB derivatives described here, which are either inactive or have very greatly reduced biological activity but are still immunoreactive, may prove to be important for the development of a protective necrotic enteritis vaccine.

MATERIALS AND METHODS

Bacterial strains and molecular techniques. Bacterial strains and plasmids are listed in Table S2 in the supplemental material and were grown as described in the supplemental material. DNA purification, PCR amplification, and DNA sequencing were carried out using standard methods that also are described in the supplemental material.

Construction of site-directed *netB* mutants. The *netB* template plasmid pJIR3618 was constructed by subcloning a 1.7-kb fragment containing the 969-bp *netB* gene region into pT7Blue. Site-directed mutagenesis was performed using the QuikChange site-directed mutagenesis kit (Qiagen), using the mutagenic primers JRP4294 and JRP4295 (for D186N) and JRP4296 and JRP4297 (for R230Q) (see Table S3 in the supplemental material). The resultant mutations were confirmed by sequence analysis, and the respective 1.7-kb *netB* fragments were subcloned into the *C. perfringens*/*Escherichia coli* shuttle plasmid pJIR1457 (41). Finally, the shuttle plasmids were introduced into derivatives of the required *C. perfringens* strains (see Table S2) by electroporation at 2.5 kV, 200 Ω, and 25 µF (42). Two additional site-directed mutants (K107A and Y108A) were constructed in the *E. coli netB*-expression vector pJIR3809.

Construction of random *netB* mutants. Random mutagenesis was carried out as previously described (43). The template plasmid (pJIR3650) containing the 1.7-kb *netB* fragment was used to transform XL1-Red competent cells (Stratagene). Plasmid DNA was extracted from the resultant pooled transformants and used to electroporate *C. perfringens* strain JIR4444, which is a nonhemolytic *plc* and *pfo* double mutant of strain JIR325 (24). Transformants were selected on HBA containing thiamphenicol to select for the presence of the shuttle plasmid. Potential *netB* mutants were screened as nonhemolytic colonies on HBA. These colonies were subcultured and subjected to PCR and sequence analysis to identify mutations in the *netB* gene region.

Expression and purification of recombinant NetB proteins. The 879-bp wild-type and mutated *netB* genes (encoding residues 31 to 322) were PCR amplified using Phusion DNA polymerase (Finnzymes) and subcloned into a pDEST plasmid encoding a C-terminal 6× His-NusA tag (His$_6$NusA) (44, 45) such that a TEV cleavage sequence was encoded immediately before the *netB* sequence. All plasmid inserts were confirmed by sequence analysis and introduced into the overexpression strain Rosetta2(DE3)pLysS (Novagen). His$_6$NusA-NetB was expressed by culturing in LB Overnight Express medium (Novagen) overnight at 28°C. Cells expressing His$_6$NusA-NetB were harvested and resuspended in buffer containing 100 mM sodium phosphate (pH 7.4) and 150 mM NaCl (PN$_{150}$ buffer). Cells were lysed by freezing and then sonication. Clarified lysate was loaded onto a HisTrap FF column (GE Healthcare Life Sciences) and equilibrated with PN$_{150}$ buffer, and the column was washed with PN$_{150}$ buffer containing 20 mM imidazole. Bound protein was eluted in batch mode using PN$_{150}$ buffer containing 500 mM imidazole. The eluate was further purified by gel filtration chromatography (Superdex200 16/60; GE Healthcare Life Sciences) using PN$_{150}$ buffer as the elution buffer. Peak fractions containing His$_6$NusA-NetB were identified by SDS-PAGE and pooled, and the His$_6$NusA tag was removed by cleavage with TEV protease (L56V/S135G derivative), which was produced as previously described (46). Briefly, for each 25 mg of fusion protein, 1 mg of His-tagged TEV protease was added and incubated at 37°C for 3 h. His$_6$NusA and uncleaved His$_6$NusA-NetB were removed by binding to a HisTrap FF column (GE Healthcare Life Sciences), which had been equilibrated with PN$_{150}$ buffer. The unbound fraction containing NetB was

collected, analyzed by SDS-PAGE, and concentrated. The substitution-containing NetB proteins were purified in a similar manner. SDS-PAGE and Western blotting were carried out by routine methods, as described in the supplemental material.

Quantitative determination of hemolytic activity. RBC were washed in PBS buffer (20 mM NaH_2PO_4, 150 mM NaCl, pH 7.4) at 4°C and diluted to an optical density of 0.5 at 595 nm in a Bio-Rad microplate reader. The washed RBC were added to serial 2-fold dilutions of the recombinant NetB protein(s) in a 96-well microtiter plate and incubated for 30 min at 37°C. The cells then were pelleted for 5 min at 3,000 $\times$ *g* at 4°C. The supernatants were removed, and their optical densities were determined at 415 nm. PBS was used as the negative control; the positive control was RBC lysed in distilled water (dH_2O).

Circular dichroism spectrometry. Circular dichroism measurements were carried out at 20°C on a Jasco J-815 CD spectrometer. NetB proteins (0.2 mg/ml) were prepared in 100 mM sodium phosphate buffer, pH 7.4, containing 0.15 M NaCl. Spectra were recorded in triplicate in the range 260 to 190 nm at a speed of 50 nm/min, with a resolution of 0.1 nm in a quartz cell with a path length of 10 nm. The data were plotted after subtraction of the spectrum of the buffer.

Crystallization and determination of crystal structure of NetB. NetB was further purified by gel filtration chromatography (PN_{150} buffer, Superdex75 16/60; GE Healthcare Life Sciences) and crystallized as described in the supplemental material, and X-ray diffraction data were collected at 100 K. The crystals diffracted to a 1.8-Å resolution and belonged to the monoclinic space group *C*2, with the following unit cell dimensions: $a = 167.4$ Å, $b = 29.7$ Å, $c = 56.3$ Å, and $\beta = 99.1°$. The data were processed and scaled using the software packages MOSFLM and SCALA (47, 48). The structure was solved by the molecular replacement method using the software program PHASER (49). The ARP/wARP, COOT, and REFMAC software programs were used to build and refine the structure (50–53). The data collection and refinement statistics are given in Table S1 in the supplemental material. These methods are described in detail in the supplemental material.

Pore formation in planar phospholipid bilayers. Pure synthetic lipids (Avanti Polar Lipids) were dispersed in chloroform and stored at −70°C under nitrogen. Briefly, lipid bilayers were formed from a dispersion of 15 mg/ml palmitoyl-oleoylphosphatidylethanolamine (PE) together with either 15 mg/ml palmitoyl-oleoylphosphatidylserine (PS) or 1,2-diphytanoyl-glycero-3-phosphocholine (PC) in *n*-decane, which was drawn across a 0.4-mm-diameter hole in a polystyrene cup separating two solution-filled chambers, designated *cis* and *trans*. The *cis* chamber, to which the toxin was added, was held at ground (0 mV), and the *trans* chamber was clamped to a range of potentials using a GeneClamp 500 patch-clamp amplifier equipped with a CV-5B (100 GΩ) bilayer headstage (Axon Instruments). The sign of the membrane potential refers to the *trans* chamber, and currents were defined as "positive" when cations flowed from *trans* to *cis*. Transmembrane currents were low-pass filtered at 100 Hz within the amplifier (8-pole Bessel) and digitized at 1 kHz directly to a computer disk via a National Instruments USB 6221 device (16-bit analogue to digital converter interface). Membrane capacitance was measured by differentiating a triangle-wave input of 0.2 kHz. Bilayers had leak currents up to 0.2 pA and a capacitance of 350 pF. Recordings were made at room temperature (19 to 22°C). Repeated 120-s recordings were made at +40 mV unless stated otherwise. Ramp protocols were carried out between ±50 mV over 5-s durations. KCl gradients were created by replacement of 50 μl 3 M KCl in the *trans* chamber. Ramps were recorded first in symmetrical 0.1 M KCl and then repeated in 0.4 M:0.1 M *trans*/*cis* KCl gradients after current had stabilized following monitoring of the current at 0 mV. Recordings were made and analyzed off-line using the WinEDR v3.2.6 software program (J. Dempster, Strathclyde Electrophysiology Software).

Protein structure accession number. The atomic coordinates and structure factor amplitudes of NetB have been deposited in the Protein Data Bank (4I0N).

SUPPLEMENTAL MATERIAL

ACKNOWLEDGMENTS

REFERENCES

1. **Gonzalez MR, Bischofberger M, Pernot L, van der Goot FG, Frêche B.** 2008. Bacterial pore-forming toxins: the (w)hole story? Cell. Mol. Life Sci. **65**:493–507.
2. **Rosado CJ, Buckle AM, Law RH, Butcher RE, Kan WT, Bird CH, Ung K, Browne KA, Baran K, Bashtannyk-Puhalovich TA, Faux NG, Wong W, Porter CJ, Pike RN, Ellisdon AM, Pearce MC, Bottomley SP, Emsley J, Smith AI, Rossjohn J, Hartland EL, Voskoboinik I, Trapani JA, Bird PI, Dunstone MA, Whisstock JC.** 2007. A common fold mediates vertebrate defense and bacterial attack. Science **317**:1548–1551.
3. **Bischofberger M, Gonzalez MR, van der Goot FG.** 2009. Membrane injury by pore-forming proteins. Curr. Opin. Cell Biol. **21**:589–595.
4. **Feil SC, Polekhina G, Gorman MA, Parker MW.** 2010. Proteins: membrane binding and pore formation. Introduction. Adv. Exp. Med. Biol. **677**:1–13.
5. **Tilley SJ, Saibil HR.** 2006. The mechanism of pore formation by bacterial toxins. Curr. Opin. Struct. Biol. **16**:230–236.
6. **Parker MW, Buckley JT, Postma JP, Tucker AD, Leonard K, Pattus F, Tsernoglou D.** 1994. Structure of the *Aeromonas* toxin proaerolysin in its water-soluble and membrane-channel states. Nature **367**:292–295.
7. **Cole AR, Gibert M, Popoff M, Moss DS, Titball RW, Basak AK.** 2004. Clostridium perfringens epsilon-toxin shows structural similarity to the pore-forming toxin aerolysin. Nat. Struct. Mol. Biol. **11**:797–798.
8. **Popoff MR.** 2011. Epsilon toxin: a fascinating pore-forming toxin. FEBS J. **278**:4602–4615.
9. **Kitadokoro K, Nishimura K, Kamitani S, Fukui-Miyazaki A, Toshima H, Abe H, Kamata Y, Sugita-Konishi Y, Yamamoto S, Karatani H, Horiguchi Y.** 2011. Crystal structure of *Clostridium perfringens* enterotoxin displays features of beta-pore-forming toxins. J. Biol. Chem. **286**:19549–19555.
10. **Song L, Hobaugh MR, Shustak C, Cheley S, Bayley H, Gouaux JE.** 1996. Structure of staphylococcal alpha-hemolysin, a heptameric transmembrane pore. Science **274**:1859–1866.
11. **Kaneko J, Kamio Y.** 2004. Bacterial two-component and heteroheptameric pore-forming cytolytic toxins: structures, pore-forming mechanism, and organization of the genes. Biosci. Biotechnol. Biochem. **68**:981–1003.
12. **Yamashita K, Kawai Y, Tanaka Y, Hirano N, Kaneko J, Tomita N, Ohta M, Kamio Y, Yao M, Tanaka I.** 2011. Crystal structure of the octameric pore of staphylococcal γ-hemolysin reveals the beta-barrel pore formation mechanism by two components. Proc. Natl. Acad. Sci. U. S. A. **108**:17314–17319.
13. **Hardy SP, Lund T, Granum PE.** 2001. CytK toxin of *Bacillus cereus* forms pores in planar lipid bilayers and is cytotoxic to intestinal epithelia. FEMS Microbiol. Lett. **197**:47–51.
14. **Nagahama M, Hayashi S, Morimitsu S, Sakurai J.** 2003. Biological

activities and pore formation of *Clostridium perfringens* beta toxin in HL 60 cells. J. Biol. Chem. **278**:36934–36941.

15. **Keyburn AL, Boyce JD, Vaz P, Bannam TL, Ford ME, Parker D, Di Rubbo A, Rood JI, Moore RJ.** 2008. NetB, a new toxin that is associated with avian necrotic enteritis caused by *Clostridium perfringens*. PLoS Pathog. **4**:e26. http://dx.doi.org/10.1371/journal.ppat.0040026.

16. **Keyburn AL, Bannam TL, Moore RJ, Rood JI.** 2010. NetB, a pore-forming toxin from necrotic enteritis strains of *Clostridium perfringens*. Toxins (Basel) **2**:1913–1927.

17. **Jayasinghe L, Miles G, Bayley H.** 2006. Role of the amino latch of staphylococcal alpha-hemolysin in pore formation: a co-operative interaction between the N terminus and position 217. J. Biol. Chem. **281**: 2195–2204.

18. **Olson R, Nariya H, Yokota K, Kamio Y, Gouaux E.** 1999. Crystal structure of staphylococcal LukF delineates conformational changes accompanying formation of a transmembrane channel. Nat. Struct. Biol. **6**:134–140.

19. **Guillet V, Roblin P, Werner S, Coraiola M, Menestrina G, Monteil H, Prevost G, Mourey L.** 2004. Crystal structure of leucotoxin S component: new insight into the staphylococcal beta-barrel pore-forming toxins. J. Biol. Chem. **279**:41028–41037.

20. **Galdiero S, Gouaux E.** 2004. High resolution crystallographic studies of alpha-hemolysin-phospholipid complexes define heptamer-lipid head group interactions: implication for understanding protein-lipid interactions. Protein Sci. **13**:1503–1511.

21. **Walker B, Bayley H.** 1995. Key residues for membrane binding, oligomerization, and pore forming activity of staphylococcal alpha-hemolysin identified by cysteine scanning mutagenesis and targeted chemical modification. J. Biol. Chem. **270**:23065–23071.

22. **Steinthorsdottir V, Fridriksdottir V, Gunnarsson E, Andrésson OS.** 1998. Site-directed mutagenesis of *Clostridium perfringens* beta-toxin: expression of wild-type and mutant toxins in *Bacillus subtilis*. FEMS Microbiol. Lett. **158**:17–23.

23. **Steinthorsdottir V, Halldórsson H, Andrésson OS.** 2000. Clostridium perfringens beta-toxin forms multimeric transmembrane pores in human endothelial cells. Microb. Pathog. **28**:45–50.

24. **Awad MM, Ellemor DM, Boyd RL, Emmins JJ, Rood JI.** 2001. Synergistic effects of alpha-toxin and perfringolysin O in *Clostridium perfringens*-mediated gas gangrene. Infect. Immun. **69**:7904–7910.

25. **Keyburn AL, Yan XX, Bannam TL, Van Immerseel F, Rood JI, Moore RJ.** 2010. Association between avian necrotic enteritis and *Clostridium perfringens* strains expressing NetB toxin. Vet. Res. **41**:21. http://dx.doi.org/10.1051/vetres/2009069.

26. **Van Immerseel F, Rood JI, Moore RJ, Titball RW.** 2009. Rethinking our understanding of the pathogenesis of necrotic enteritis in chickens. Trends Microbiol. **17**:32–36.

27. **Menestrina G.** 1986. Ionic channels formed by *Staphylococcus aureus* alpha-toxin: voltage-dependent inhibition by divalent and trivalent cations. J. Membr. Biol. **90**:177–190.

28. **Cooper KK, Songer JG.** 2009. Necrotic enteritis in chickens: a paradigm of enteric infection by *Clostridium perfringens* type A. Anaerobe **15**:55–60.

29. **Timbermont L, Haesebrouck F, Ducatelle R, Van Immerseel F.** 2011. Necrotic enteritis in broilers: an updated review on the pathogenesis. Avian Pathol. **40**:341–347.

30. **Bokori-Brown M, Savva CG, Fernandes da Costa SP, Naylor CE, Basak AK, Titball RW.** 2011. Molecular basis of toxicity of *Clostridium perfringens* epsilon toxin. FEBS J. **278**:4589–4601.

31. **Briggs DC, Naylor CE, Smedley JG, III, Lukoyanova N, Robertson S, Moss DS, McClane BA, Basak AK.** 2011. Structure of the food-poisoning *Clostridium perfringens* enterotoxin reveals similarity to the aerolysin-like pore-forming toxins. J. Mol. Biol. **413**:138–149.

32. **Krasilnikov OV, Merzlyak PG, Yuldasheva LN, Rodrigues CG, Bhakdi S, Valeva A.** 2000. Electrophysiological evidence for heptameric stoichiometry of ion channels formed by *Staphylococcus aureus* alpha-toxin in planar lipid bilayers. Mol. Microbiol. **37**:1372–1378.

33. **Shatursky O, Bayles R, Rogers M, Jost BH, Songer JG, Tweten RK.** 2000. Clostridium perfringens beta-toxin forms potential-dependent, cation-selective channels in lipid bilayers. Infect. Immun. **68**:5546–5551.

34. **Manich M, Knapp O, Gibert M, Maier E, Jolivet-Reynaud C, Geny B, Benz R, Popoff MR.** 2008. Clostridium perfringens delta toxin is sequence related to beta toxin, NetB, and *Staphylococcus* pore-forming toxins, but shows functional differences. PLoS One **3**:e3764. http://dx.doi.org/10.1371/journal.pone.0003764.

35. **Savva CG, Fernandes da Costa SP, Bokori-Brown M, Naylor CE, Cole AR, Moss DS, Titball RW, Basak AK.** 13 December 2012. Molecular architecture and functional analysis of NetB, a pore-forming toxin from *Clostridium perfringens*. J. Biol. Chem. http://www.jbc.org/cgi/doi/10.1074/jbc.M112.430223.

36. **Nelson GJ.** 1967. Composition of neutral lipids from erythrocytes of common mammals. J. Lipid Res. **8**:374–379.

37. **Beach DH, Sherman IW, Holz GG, Jr.** 1977. Lipids of *Plasmodium lophurae*, and of erythrocytes and plasma of normal and *P. lophurae*-infected Pekin ducklings. J. Parasitol. **63**:62–75.

38. **Kulkarni RR, Parreira VR, Sharif S, Prescott JF.** 2007. Immunization of broiler chickens against *Clostridium perfringens*-induced necrotic enteritis. Clin. Vaccine Immunol. **14**:1070–1077.

39. **Zekarias B, Mo H, Curtiss R, III.** 2008. Recombinant attenuated *Salmonella enterica* serovar Typhimurium expressing the carboxy-terminal domain of alpha toxin from *Clostridium perfringens* induces protective responses against necrotic enteritis in chickens. Clin. Vaccine Immunol. **15**:805–816.

40. **Jang SI, Lillehoj HS, Lee SH, Lee KW, Lillehoj EP, Hong YH, An DJ, Jeong W, Chun JE, Bertrand F, Dupuis L, Deville S, Arous JB.** 2012. Vaccination with *Clostridium perfringens* recombinant proteins in combination with Montanide ™ ISA 71 VG adjuvant increases protection against experimental necrotic enteritis in commercial broiler chickens. Vaccine **30**:5401–5406.

41. **Lyras D, Rood JI.** 1998. Conjugative transfer of RP4-*oriT* shuttle vectors from *Escherichia coli* to *Clostridium perfringens*. Plasmid **39**:160–164.

42. **Scott PT, Rood JI.** 1989. Electroporation-mediated transformation of lysostaphin-treated *Clostridium perfringens*. Gene **82**:327–333.

43. **Bannam TL, Rood JI.** 1999. Identification of structural and functional domains of the tetracycline efflux protein TetA(P) from *Clostridium perfringens*. Microbiology **145**:2947–2955.

44. **Cabrita LD, Dai W, Bottomley SP.** 2006. A family of *E. coli* expression vectors for laboratory scale and high throughput soluble protein production. BMC Biotechnol. **6**:12. http://dx.doi.org/10.1186/1472-6750-6-12.

45. **Braud S, Moutiez M, Belin P, Abello N, Drevet P, Zinn-Justin S, Courçon M, Masson C, Dassa J, Charbonnier JB, Boulain JC, Ménez A, Genet R, Gondry M.** 2005. Dual expression system suitable for high-throughput fluorescence-based screening and production of soluble proteins. J. Proteome Res. **4**:2137–2147.

46. **Cabrita LD, Gilis D, Robertson AL, Dehouck Y, Rooman M, Bottomley SP.** 2007. Enhancing the stability and solubility of TEV protease using in silico design. Protein Sci. **16**:2360–2367.

47. **Evans P.** 2006. Scaling and assessment of data quality. Acta Crystallogr. D Biol. Crystallogr. **62**:72–82.

48. **Leslie AGW.** 1992. Recent changes to the MOSFLM package for processing film and image plate data. Joint CCP4 + ESF-EAMCB. Newsl. Proteins Crystallogr. **26**:27–33.

49. **McCoy AJ, Grosse-Kunstleve RW, Adams PD., Winn MD, Storoni LC, Read RJ.** 2007. Phaser crystallographic software. J. Appl. Crystallogr. **40**: 658–674.

50. **Emsley P, Cowtan K.** 2004. Coot: model-building tools for molecular graphics. Acta Crystallogr. D Biol. Crystallogr. **60**:2126–2132.

51. **Murshudov GN, Vagin AA, Dodson EJ.** 1997. Refinement of macromolecular structures by the maximum-likelihood method. Acta Crystallogr. D Biol. Crystallogr. **53**:240–255.

52. **Collaborative Computational Project, Number 4.** 1994. The CCP4 suite: programs for protein crystallography. Acta Crystallogr. D Biol. Crystallogr. **50**:760–763.

53. **Langer G, Cohen SX, Lamzin VS, Perrakis A.** 2008. Automated macromolecular model building for X-ray crystallography using ARP/wARP version 7. Nat. Protoc. **3**:1171–1179.

54. **Pédelacq JD, Maveyraud L, Prévost G, Baba-Moussa L, González A, Courcelle E, Shepard W, Monteil H, Samama JP, Mourey L.** 1999. The structure of a *Staphylococcus aureus* leucocidin component (LukF-PV) reveals the fold of the water-soluble species of a family of transmembrane pore-forming toxins. Structure **7**:277–287.